

# Bulk Assembly of Corrugated 1D Metal Halides with Broadband Yellow Emission

Haoran Lin, Chenkun Zhou, Jennifer Neu, Yan Zhou, Dan Han, Shiyu Chen, Michael Worku, Maya Chaaban, Sujin Lee, Ella Berkwits, Theo Siegrist,\* Mao-Hua Du,\* and Biwu Ma\*

The family of molecular level low-dimensional organic metal halide hybrids has expanded significantly over the last few years. Here a new type of 1D metal halide structure is reported, in which metal halide octahedra form a corrugated double-chain structure via nonplanar edge-sharing. This material with a chemical formula of  $C_5H_{16}N_2Pb_2Br_6$  exhibits a broadband yellow emission under ultraviolet light excitation with a photoluminescence quantum efficiency of around 10%. The light-yellow emission is considered to be attributed to self-trapping excitons. Theoretical calculations show that the unique alignment of the octahedra leads to small band dispersion and large exciton binding energy. Together with previously reported 1D metal halide wires and tubes, this new bulk assembly of 1D metal halides suggests the potential to develop a library of bulk assemblies of metal halides with controlled structures and compositions.

Organic metal halide hybrids, an emerging class of functional materials, have received tremendous research interests recently.<sup>[1]</sup> One significant scientific achievement in this field is the synthetic control of dimensionality of this class of materials at the molecular level. By assembling appropriate organic and metal halide components, organic metal halide hybrids with layered<sup>[2]</sup> and corrugated 2D structures,<sup>[3]</sup> 1D wire<sup>[4]</sup> and tubular structures,<sup>[5]</sup> and 0D molecular<sup>[6]</sup> and cluster structures,<sup>[7]</sup> have been developed to exhibit properties significantly different from those of 3D  $ABX_3$  metal halide perovskites. The unique photophysical properties of these molecular level low-dimensional organic metal halide hybrids are mainly attributed to the high degree of structural distortion and strong quantum confinement effect.<sup>[8]</sup> As a result, different radiative decay mechanisms involving either free excitonic states or self-trapped states exist in these hybrid materials.<sup>[9]</sup> The presence of self-trapped excited states could lead to broadband emissions with large Stokes shifts, which are of interest for a variety of optoelectronic applications, such as light-emitting devices and luminescent solar concentrators.

Despite the advance of organic metal halide hybrids from 3D to 2D, 1D, and 0D at the molecular level during the last couple of years, the research in this field is still in the early stage with a relatively small number of low dimensional organic metal halide hybrids reported to date. Nevertheless, the limited number of examples has already demonstrated the exceptional structural tunability of these materials. For instance, it was found that metal halide octahedra can be connected by corner-sharing,<sup>[10]</sup> edge-sharing,<sup>[4b,11]</sup> face-sharing<sup>[4a]</sup> or combinations<sup>[5b,12]</sup> to form linear, zig-zag, bilinear, or even tubular 1D structures. This suggests that there is ample room for further exploring the composition, size, and morphology of bulk assemblies of low-dimensional organic metal halide hybrids with novel structures and functionalities. Motivated by the previous success in controlling quantum confinement as well as the optical and electronic properties in morphological 1D inorganic nanowires,<sup>[13]</sup> we have carried out research on developing new bulk assemblies of 1D metal halides with the width of the metal halide wire/chain exceeding that of a single octahedron. This enables us to expand the structure–property space of this family of hybrid materials for more effective property tuning and novel functionalities.

Dr. H. Lin, Y. Zhou, M. Chaaban, S. Lee, Prof. B. Ma  
Department of Chemistry and Biochemistry  
Florida State University  
Tallahassee, FL 32306, USA  
E-mail: bma@fsu.edu

C. Zhou, E. Berkwits, Prof. T. Siegrist  
Department of Chemical and Biomedical Engineering  
FAMU-FSU College of Engineering  
Tallahassee, FL 32310, USA  
E-mail: tsiegrist@fsu.edu

J. Neu, Prof. T. Siegrist  
National High Magnetic Field Laboratory  
Florida State University  
Tallahassee, FL 32310, USA

D. Han, Dr. M.-H. Du  
Materials Science and Technology Division  
Oak Ridge National Laboratory  
Oak Ridge, TN 37831, USA  
E-mail: mhdu@ornl.gov

Prof. S. Chen  
Department of Physics  
East China Normal University  
Shanghai 200241, China

M. Worku, Prof. B. Ma  
Materials Science and Engineering Program  
Florida State University  
Tallahassee, FL 32306, USA

 The ORCID identification number(s) for the author(s) of this article can be found under <https://doi.org/10.1002/adom.201801474>.

DOI: 10.1002/adom.201801474

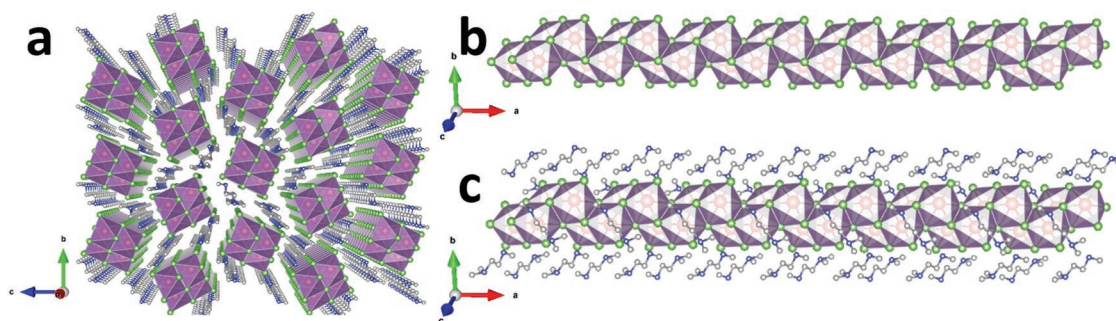


**Figure 1.** a) Crystal structure of  $C_5H_{16}N_2Pb_2Br_6$  (red: lead atoms; green: bromine atoms; blue: nitrogen atoms; gray: carbon atoms; purple polyhedron:  $PbBr_6$  octahedra; hydrogen atoms were hidden for clarity). b) Side view of an individual lead bromide double chain. c) Side view of an individual lead bromide double chain with the organic cations.

Here we report a new 1D organic metal halide hybrid,  $C_5H_{16}N_2Pb_2Br_6$  (TMEDAPb $_2$ Br $_6$ ), in which corrugated-1D double-chain metal halide nanowires ( $Pb_2Br_6$ ) $^{2-}$  are separated by the large bandgap organic cations (*N,N,N'*-trimethylethylenediammonium, TMEDA $^{2+}$ ). The “1D” herein is defined as molecular level 1D nanostructure within the bulk-assembly crystal.<sup>[14]</sup> As observed in other molecular level low dimensional organic metal halide hybrids, the site isolation between the double-chain nanowires enables the bulk crystals to exhibit the intrinsic properties of the individual nanowires.<sup>[15]</sup> A strongly Stokes-shifted light-yellow emission peaked at 554 nm with a large full width at half maximum (FWHM) of 155 nm and a photoluminescence quantum efficiency (PLQE) of around 10% was observed. Density functional theory (DFT) calculations found that the dispersion of both the valence and conduction bands is small even along the direction of the nanowire as a result of the nonplanar edge-sharing, and that the emission is from the self-trapped exciton (STE) with the hole and the electron localized at the adjacent  $Pb^{3+}$  and  $Pb_2^{3+}$  sites, respectively, in the metal halide framework.

Single crystalline  $C_5H_{16}N_2Pb_2Br_6$  was prepared via slow vapor diffusion of diethyl ether into hydrobromic acid solution of *N,N,N'*-trimethylethylenediamine dihydrobromide (TME-DABr $_2$ ) and lead bromide ( $PbBr_2$ ) (see the experimental details in the Supporting Information). Single crystal X-ray diffraction (SCXRD) was used to characterize its structure (Tables S1 and S2, Supporting Information). The powder X-ray diffraction experiment was also carried out for the grounded  $C_5H_{16}N_2Pb_2Br_6$  powders to confirm the SCXRD results (Figure S2, Supporting Information). **Figure 1a** shows the front view of the bulk assembly crystal structure facing the direction of the metal halide nanowire arrays. **Figure 1b,c** shows the side views of an individual lead bromide double chain composed by  $PbBr_6$  octahedra without and with organic cations, respectively. Along the growth direction of an individual 1D nanostructure, the octahedra first share two noncoplanar edges with two adjacent octahedra to form a 1D zig-zag chain (**Figure 1b** front part), then the second chain (**Figure 1b** back part) slide and stack together with the first chain, connected also through edge-sharing. Therefore, the 1D metal halide nanowire can be regarded as a corrugated-1D double chain structure. This connecting arrangement of sharing noncoplanar edges is rarely reported for 1D metal halide hybrids.<sup>[11a,16]</sup> Moreover, compared with the edge-sharing single chain 1D metal halide hybrids with a general formula of  $ABX_4$  (in which A stands for divalent organic cations, B stands for divalent metal cations, and X for

halides), the increase of the B:X ratio from 1:4 in  $ABX_4$  to 1:3 in  $C_5H_{16}N_2Pb_2Br_6$  indicates that the lead bromide octahedra in  $C_5H_{16}N_2Pb_2Br_6$  share more Br atoms and are thus more “condensed.” As a result, the coordination numbers of Br atoms in  $C_5H_{16}N_2Pb_2Br_6$  increase up to 4 (The coordination number of Br atoms are 1, 2 to 4). The different environments for the bromine atoms result in varied Pb–Br bond lengths from 2.811 to 3.340 Å and varied Br–Pb–Br bond angles from 81.68° to 98.59° (Tables S3 and S4, Supporting Information). The distorted octahedra within the 1D lead bromide wire should be favorable for the excitonic state structural deformation and the formation of self-trapped excitonic states. As shown in **Figure 1a,c**, the double chain arrays are surrounded and isolated by the bulky organic cations; therefore, no significant interchain electronic interaction is expected (confirmed by the DFT calculation below).  $C_5H_{16}N_2Pb_2Br_6$  can therefore be viewed as the bulk assembly of core–shell quantum wires exhibiting the intrinsic properties of corrugated-1D lead bromide chains.

We further characterized the thermal and optical properties of  $C_5H_{16}N_2Pb_2Br_6$ . Although  $C_5H_{16}N_2Pb_2Br_6$  has a large degree of structural distortion (Table S5, Supporting Information), it has a high decomposition temperature of 270 °C determined by thermogravimetric analysis (**Figure S3**, Supporting Information). Moreover, almost no change of the PL spectrum occurred after leaving this material in air for six months (**Figure S4**, Supporting Information), suggesting good stability of this material for its potential application in devices working under harsh conditions. The photophysical properties of  $C_5H_{16}N_2Pb_2Br_6$  were characterized by static and time-resolved photoluminescence spectroscopies. As shown in **Figure 2a**,  $C_5H_{16}N_2Pb_2Br_6$  single crystals are colorless under ambient light and exhibit light yellow emission under illumination of ultraviolet (UV) radiation (365 nm), suggesting a below-gap broadband emission with large Stokes shift. The excitation spectrum shows that  $C_5H_{16}N_2Pb_2Br_6$  can be excited by UV light from 250 to 390 nm. The absorption spectrum is generally in accordance with the excitation, and the absorption onset of around 400 nm suggests an optical bandgap of around 3.1 eV. The broadband emission of  $C_5H_{16}N_2Pb_2Br_6$  covers the whole spectrum of visible light from 400 to 750 nm with a single peak located at around 554 nm and an FWHM of 155 nm (**Figure 2b**). We also observed similar emission spectra obtained with three different excitation wavelengths (330, 360, and 380 nm), indicating the excitation-independent property of the emission (**Figure S5**, Supporting Information). The Commission

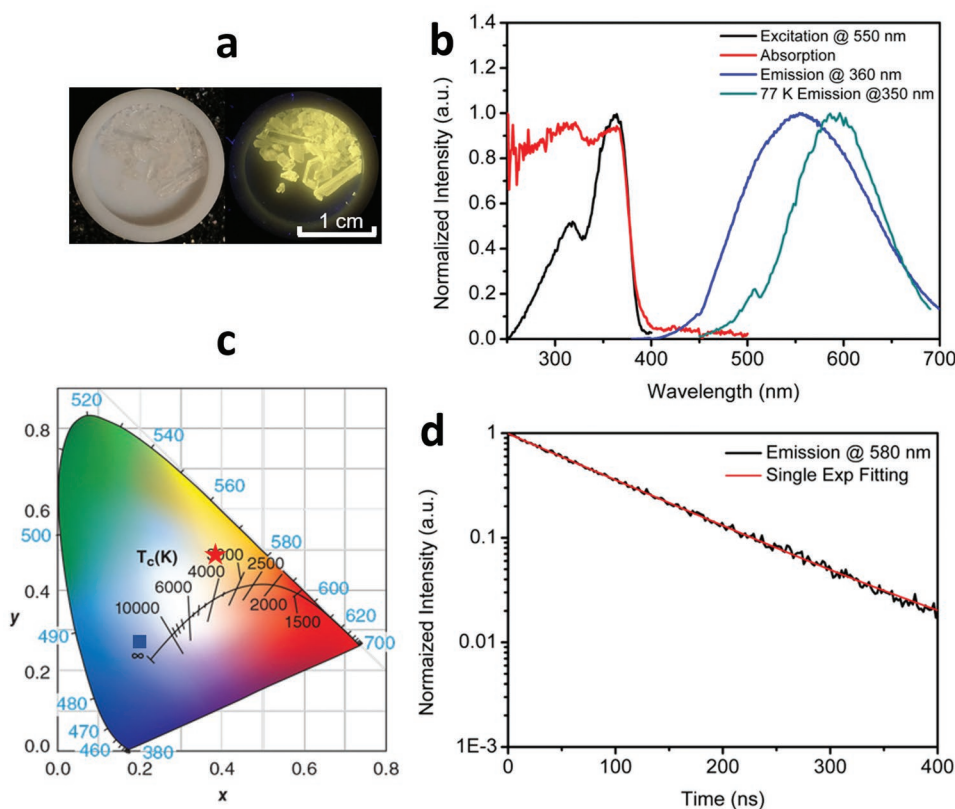


**Figure 2.** a) Images of  $C_5H_{16}N_2Pb_2Br_6$  crystals under ambient light (left) and UV light (365 nm, right). b) Excitation (black line, probed at 550 nm), absorption (red line), room temperature emission (blue line, excited by 360 nm UV light), and 77 K emission (dark cyan line, excited by 350 nm UV light) spectra of  $C_5H_{16}N_2Pb_2Br_6$  crystals. c) CIE chromaticity coordinates of the emissions from  $C_5H_{16}N_2Pb_2Br_6$  (red star) and  $C_4H_{14}N_2PbBr_4$  (blue square, ref. [11]). d) Time-resolved PL decay and its single-exponential fitting of  $C_5H_{16}N_2Pb_2Br_6$  crystals (excited by 365 nm diode laser, probed at 580 nm) at room temperature.

Internationale de l'Éclairage (CIE) chromaticity coordinates for this light-yellow emission are calculated to be (0.38, 0.48) with a color rendering index (CRI) value of 67, falling in the region of “warm white light” (Figure 2c). Compared with our previously reported blue-emitting edge-sharing 1D  $C_4H_{14}N_2PbBr_4$ ,<sup>[4b]</sup> the light-yellow emission of  $C_5H_{16}N_2Pb_2Br_6$  is significantly red-shifted. The large Stokes shift of  $C_5H_{16}N_2Pb_2Br_6$  also indicates strong spontaneous excited-state relaxation, which suppresses the direct band-to-band transition. The PLQE of  $C_5H_{16}N_2Pb_2Br_6$  bulk crystals is measured to be around 10%, comparable with other emissive bulk assemblies of 1D metal halides.<sup>[4b,5b]</sup> The decay lifetime was determined to be 98 ns by single-exponential fitting of the emission decay curve (Figure 2d, the functional formula of the fitting curve is specified in the Supporting Information). With the temperature lowered to 77 K, its photoluminescence remained excitation independent (Figure S6, Supporting Information), while the emission peak red-shifted to 595 nm, with a significantly reduced FWHM of 110 nm (Figure 2b). The average decay lifetime at 77 K also increased to 3.2  $\mu$ s (Figure S7, Supporting Information, the functional formulas are specified in the Supporting Information). To rule out the possibility of defect emission, we have measured the dependence of PL intensity on the excitation power density. As shown in Figure S8 in the Supporting Information, the intensity of emission excited

at 360 nm showed a linear dependence on the excitation power density up to 3.6  $MW\ cm^{-2}$ . This indicates that the emission is intrinsic rather than from defects which usually will give a saturated emission under such high excitation power density. All these results are very similar to the STE emission characteristics of previously reported corrugated-2D and 1D organic metal halide hybrids,<sup>[4c,17]</sup> suggesting that the broadband emission with large Stokes shift is the result of the radiative decay of STEs.

To gain a better understanding of the mechanism underlying the optical properties of this 1D material, we performed DFT calculations to obtain its electronic band structure and the properties of the self-trapped exciton. The calculated electronic structure of  $C_5H_{16}N_2Pb_2Br_6$  (Figure 3) shows that the valence (conduction) band is made up of antibonding states of Br-4p and Pb-6s (Pb-6p) (Figure 3b). The band dispersion is negligible in the directions perpendicular to the 1D lead bromide chain, indicating extremely weak interchain electronic coupling. Interestingly, both the valence and conduction bands have small dispersion even along the 1D chain direction. This is likely due to the structure of the 1D chain, in which no Pb–Br bonds are parallel to the chain direction and, as such, there is not an undisturbed linear Pb–Br–Pb bonding network connecting the Pb ions aligned along the chain direction. In comparison, our previously reported 1D metal halide hybrid  $C_4H_{14}N_2PbCl_4$

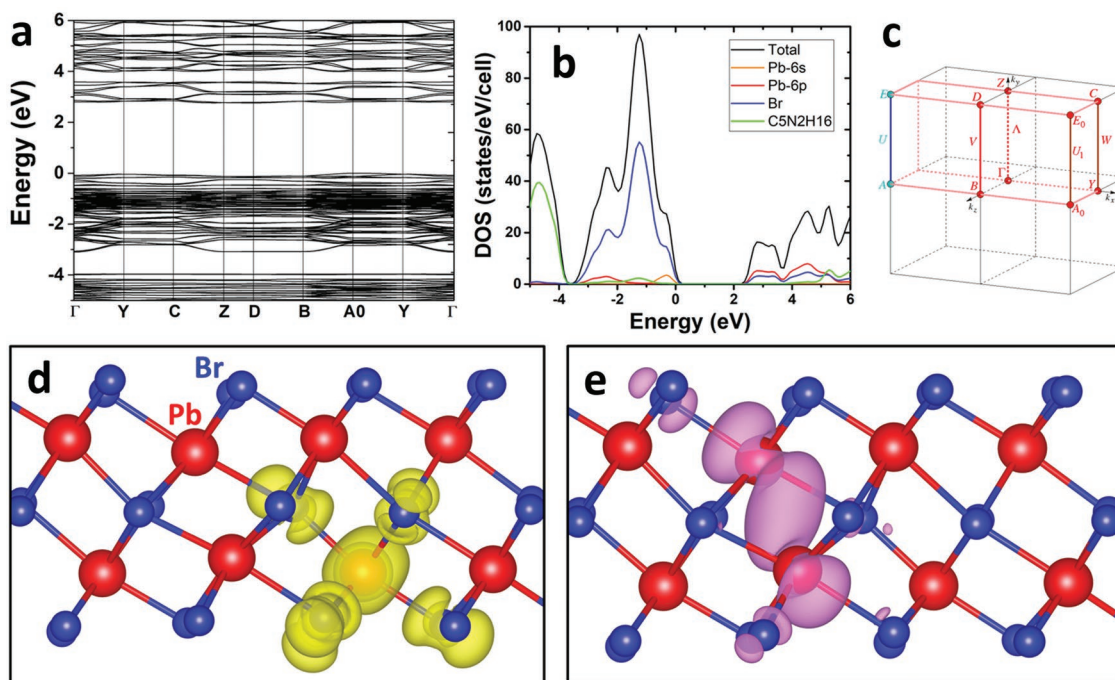


**Figure 3.** a) Electronic band structure and b) density of states of 1D  $C_5N_2H_{16}Pb_2Br_6$  calculated using the PBE functional (including the spin–orbit coupling). c) The high-symmetry  $k$  points in the Brillouin zone that are included in the band structure. Partial charge density contours of d) the hole and e) the electron wavefunctions of the self-trapped exciton in 1D  $C_5N_2H_{16}Pb_2Br_6$ . The charge densities on the isodensity surfaces of the hole and electron are 0.0003 and 0.001  $e \text{ bohr}^{-3}$ , respectively.

has the linear  $-Pb-Cl-Pb-Cl-Pb-$  bonding network running parallel to the 1D chain direction; thereby, exhibiting dispersive bands along the chain direction.<sup>[18]</sup> The bandgap of  $C_5N_2H_{16}Pb_2Br_6$  is slightly indirect. The valence band maximum is located at the A0 point while the conduction band minimum is at the D point (Figure 3a). The calculated indirect bandgap is 2.76 eV at the Perdew–Burke–Ernzerhof (PBE) level, which should be underestimated due to the well-known PBE bandgap error. The PBE0 calculation increases the bandgap to 4.43 eV.

The PBE0 calculation (including spin–orbit coupling) shows that the excitation of an exciton in  $C_5H_{16}N_2Pb_2Br_6$  involves the promotion of an electron from the Pb-6s orbital to the Pb-6p orbitals at a single sixfold-coordinated  $Pb^{2+}$  ion. The calculated excitation energy is 3.53 eV (351 nm), within the excitation band observed in experiment (Figure 2b). The calculated exciton excitation energy is significantly smaller than the calculated bandgap (4.43 eV), indicating strong electron–hole Coulomb binding at the localized exciton. The excited-state structural relaxation lowers the total energy by 0.38 eV and leads to the formation of the STE with its structure shown in Figure 3d,e. The hole is mainly centered at a Pb ion (Figure 3d) causing the contraction of the six Pb–Br bonds from 3.04 to 2.87 Å (in average). The electron is mainly trapped by the two Pb ions adjacent to the hole-trapping Pb ion (Figure 3e). The distance between the two Pb ions is shortened from 4.49 to 3.71 Å to trap the electron. Such self-trapped electron at the  $Pb_2^{3+}$  dimer has been observed in layered  $PbBr_2$ .<sup>[19]</sup> The calculated large binding energy of the STE, i.e., 1.28 eV, (relative to the free electron and hole) suggests that the free electrons and holes do not exist at room temperature, which explains the absence of direct

band-to-band emission. The PBE0-calculated exciton emission energy is 1.97 eV, in excellent agreement with the experimentally observed peak centered at 2.08 eV (measured at 77 K). (Note that all the DFT calculations are based on the crystal structure measured at 100 K.) The excellent agreement between the calculated exciton excitation and emission energies and the observed excitation and emission peak energies show that optical absorption onset (shown in Figure 2b) should be due to the excitonic absorption and that the light-yellow emission is due the STE.

Compared with the previously studied 1D edge-sharing materials, there are several unique characteristics for 1D  $C_5H_{16}N_2Pb_2Br_6$ . First, due to the special corrugated-1D structure, no Pb–Br bond is parallel to the direction of the nanowire growth, which means the lack of  $-Pb-Br-Pb-Br-Pb-$  bonding network along the double chain direction. Therefore, even though  $C_5H_{16}N_2Pb_2Br_6$  employs the same edge-sharing connection method as some other 1D materials, its electronic band structure and excited states are significantly affected by the orientation and stacking of the octahedra, resulting in weaker intrachain electronic interaction and larger self-trapped exciton binding energy for  $C_5H_{16}N_2Pb_2Br_6$ . (The calculated STE binding energy in 1D  $C_5H_{16}N_2Pb_2Br_6$  (1.28 eV) is significantly larger than that in 1D  $C_4H_{14}N_2PbBr_4$  (0.76 eV), which has stronger intrachain electronic coupling.) Second, 1D  $C_5H_{16}N_2Pb_2Br_6$  studied in this work has a larger width of the inorganic wire than those previously reported (expanded from single chain to double chain), demonstrating that we can synthetically control the size of the nanowire in this class of 1D organic metal halide hybrids. This provides additional means of property tuning (i.e., bandgap tuning, color tuning, etc.) via quantum confinement effect and

paves the way for developing bulk assemblies of 1D metal halides that bridge the molecular 1D and morphological 1D materials. Third, the high stability of this material indicates that ionically bonded organic–inorganic hybrids could be as stable as conventional materials to meet the requirements for stable devices.

In summary, we have prepared a novel organic metal halide hybrid material composed of isolated arrays of corrugated-1D lead bromide double chains via a simple crystallization process. Our discovery of this unique 1D structure and its corresponding properties shows once again the structural versatility of organic metal halide hybrids. On-going research aims to achieve synthetic control of the diameter and configuration of the 1D metal halide nanowires in bulk assemblies and develop theories to guide the preparation of organic metal halide hybrids with desired structures and properties.

## Supporting Information

Supporting Information is available from the Wiley Online Library or from the author.

## Acknowledgements

The authors acknowledge the support from the National Science Foundation (DMR-1709116) and the Air Force Office of Scientific Research (AFOSR) (17RT0906). J.N. and T.S. acknowledge funding from the National Science Foundation under grant DMR-606952. Part of the work was carried out at the National High Magnetic Field Laboratory, which was funded by the National Science Foundation under DMR-1644779 and the State of Florida. The work at Oak Ridge National Laboratory (ORNL) was supported by the U. S. Department of Energy, Office of Science, Basic Energy Sciences, Materials Sciences, and Engineering Division. D.H. and S.C. were supported by National Natural Science Foundation of China (NSFC) under Grant Nos. 61574059 and 61722402, Shu-Guang program (15SG20). The authors thank Dr. Kenneth Hanson at FSU for the access to a spectrophotometer.

## Conflict of Interest

The authors declare no conflict of interest.

## Keywords

1D structures, exciton self-trapping, organic metal halide hybrids, photoluminescence, quantum confinement effect

Received: October 28, 2018

Revised: January 2, 2019

Published online: January 15, 2019

- [1] a) J. S. Manser, J. A. Christians, P. V. Kamat, *Chem. Rev.* **2016**, *116*, 12956; b) P. Chen, Y. Bai, M. Q. Lyu, J. H. Yun, M. M. Hao, L. Z. Wang, *Sol. RRL* **2018**, *2*, 1700186; c) H. R. Lin, C. K. Zhou, Y. Tian, T. Siegrist, B. W. Ma, *ACS Energy Lett.* **2018**, *3*, 54.
- [2] a) L. Dou, A. B. Wong, Y. Yu, M. Lai, N. Kornienko, S. W. Eaton, A. Fu, C. G. Bischak, J. Ma, T. Ding, N. S. Ginsberg, L. W. Wang, A. P. Alivisatos, P. Yang, *Science* **2015**, *349*, 1518; b) L. N. Quan, M. Yuan, R. Comin, O. Voznyy, E. M. Beauregard, S. Hoogland, A. Buin, A. R. Kirmani, K. Zhao, A. Amassian, D. H. Kim, E. H. Sargent, *J. Am. Chem. Soc.* **2016**, *138*, 2649; c) L. Mao, W. Ke, L. Pedesseau, Y. Wu, C. Katan, J. Even, M. R. Wasielewski, C. C. Stoumpos, M. G. Kanatzidis, *J. Am. Chem. Soc.* **2018**, *140*, 3775.
- [3] a) E. R. Dohner, E. T. Hoke, H. I. Karunadasa, *J. Am. Chem. Soc.* **2014**, *136*, 1718; b) L. Mao, Y. Wu, C. C. Stoumpos, M. R. Wasielewski, M. G. Kanatzidis, *J. Am. Chem. Soc.* **2017**, *139*, 5210; c) O. Nazarenko, M. R. Kotyba, S. Yakunin, M. Aebli, G. Raino, B. M. Benin, M. Worle, M. V. Kovalenko, *J. Am. Chem. Soc.* **2018**, *140*, 3850.
- [4] a) Z. Tang, A. M. Guloy, *J. Am. Chem. Soc.* **1999**, *121*, 452; b) Z. Yuan, C. Zhou, Y. Tian, Y. Shu, J. Messier, J. C. Wang, L. J. van de Burgt, K. Kountouriotis, Y. Xin, E. Holt, K. Schanze, R. Clark, T. Siegrist, B. Ma, *Nat. Commun.* **2017**, *8*, 14051; c) Y. Peng, Y. Yao, L. Li, Z. Wu, S. Wang, J. Luo, *J. Mater. Chem. C* **2018**, *6*, 6033.
- [5] a) G. E. Wang, G. Xu, B. W. Liu, M. S. Wang, M. S. Yao, G. C. Guo, *Angew. Chem., Int. Ed.* **2016**, *55*, 514; b) H. Lin, C. Zhou, Y. Tian, T. Besara, J. Neu, T. Siegrist, Y. Zhou, J. Bullock, K. S. Schanze, W. Ming, M. H. Du, B. Ma, *Chem. Sci.* **2017**, *8*, 8400.
- [6] a) Z. P. Wang, J. Y. Wang, J. R. Li, M. L. Feng, G. D. Zou, X. Y. Huang, *Chem. Commun.* **2015**, *51*, 3094; b) L. J. Xu, C. Z. Sun, H. Xiao, Y. Wu, Z. N. Chen, *Adv. Mater.* **2017**, *29*, 1605739; c) C. K. Zhou, H. R. Lin, Y. Tian, Z. Yuan, R. Clark, B. H. Chen, L. J. van de Burgt, J. C. Wang, Y. Zhou, K. Hanson, Q. J. Meisner, J. Neu, T. Besara, T. Siegrist, E. Lambers, P. Djurovich, B. W. Ma, *Chem. Sci.* **2018**, *9*, 586.
- [7] a) G. Giorgi, K. Yamashita, *J. Phys. Chem. Lett.* **2016**, *7*, 888; b) W. Liu, K. Zhu, S. J. Teat, G. Dey, Z. Shen, L. Wang, D. M. O'Carroll, J. Li, *J. Am. Chem. Soc.* **2017**, *139*, 9281.
- [8] a) T. Hu, M. D. Smith, E. R. Dohner, M. J. Sher, X. Wu, M. T. Trinh, A. Fisher, J. Corbett, X. Y. Zhu, H. I. Karunadasa, A. M. Lindenberg, *J. Phys. Chem. Lett.* **2016**, *7*, 2258; b) D. Cortecchia, S. Neutzner, A. R. Srimath Kandada, E. Mosconi, D. Meggiolaro, F. De Angelis, C. Soci, A. Petrozza, *J. Am. Chem. Soc.* **2017**, *139*, 39.
- [9] a) X. Wu, M. T. Trinh, D. Niesner, H. Zhu, Z. Norman, J. S. Owen, O. Yaffe, B. J. Kudisch, X. Y. Zhu, *J. Am. Chem. Soc.* **2015**, *137*, 2089; b) D. Han, H. L. Shi, W. M. Ming, C. K. Zhou, B. W. Ma, B. Saparov, Y. Z. Ma, S. Y. Chen, M. H. Du, *J. Mater. Chem. C* **2018**, *6*, 6398.
- [10] a) G. A. Mousdis, V. Gionis, G. C. Papavassiliou, C. P. Raptopoulou, A. Terzis, *J. Mater. Chem.* **1998**, *8*, 2259; b) C. P. Raptopoulou, A. Terzis, G. A. Mousdis, G. C. Papavassiliou, *Z. Naturforsch. B* **2002**, *57*, 645.
- [11] a) T. Y. Li, Y. Hu, C. A. Morrison, W. J. Wu, H. W. Han, N. Robertson, *Sustainable Energy Fuels* **2017**, *1*, 308; b) M. E. Kammaing, G. A. de Wijs, R. W. A. Havenith, G. R. Blake, T. T. M. Palstra, *Inorg. Chem.* **2017**, *56*, 8408.
- [12] L. Mao, P. Guo, M. Kepenekian, I. Hadar, C. Katan, J. Even, R. D. Schaller, C. C. Stoumpos, M. G. Kanatzidis, *J. Am. Chem. Soc.* **2018**, *140*, 13078.
- [13] M. Imran, F. Di Stasio, Z. Y. Dang, C. Canale, A. H. Khan, J. Shamsi, R. Brescia, M. Prato, L. Manna, *Chem. Mater.* **2016**, *28*, 6450.
- [14] C. Zhou, H. Lin, Q. He, L. Xu, M. Worku, M. Chaaban, S. Lee, X. Shi, M.-H. Du, B. Ma, *Mater. Sci. Eng., R* **2019**, *137*, 38.
- [15] C. Zhou, H. Lin, S. Lee, M. Chaaban, B. Ma, *Mater. Res. Lett.* **2018**, *6*, 552.
- [16] Y. Li, G. Zheng, C. Lin, J. Lin, *Solid State Sci.* **2007**, *9*, 855.
- [17] a) Z. Yuan, C. K. Zhou, J. Messier, Y. Tian, Y. Shu, J. M. Wang, Y. Xin, B. W. Ma, *Adv. Opt. Mater.* **2016**, *4*, 2009; b) Z. Y. Wu, C. M. Ji, Z. H. Sun, S. S. Wang, S. G. Zhao, W. C. Zhang, L. N. Li, J. H. Luo, *J. Mater. Chem. C* **2018**, *6*, 1171.
- [18] G. H. Wu, C. K. Zhou, W. M. Ming, D. Han, S. Y. Chen, D. Yang, T. Besara, J. Neu, T. Siegrist, M. H. Du, B. W. Ma, A. G. Dong, *ACS Energy Lett.* **2018**, *3*, 1443.
- [19] a) S. V. Nistor, E. Goovaerts, D. Schoemaker, *Phys. Rev. B* **1993**, *48*, 9575; b) M. Iwanaga, J. Azuma, M. Shirai, K. Tanaka, T. Hayashi, *Phys. Rev. B* **2002**, *65*, 214306.